Seasonal prediction skill of East Asian summer monsoon in CMIP5-Models

Bo Huang,* Ulrich Cubasch, Christopher Kadow

Institute of Meteorology, Freie Universität Berlin,
Carl-Heinrich-Becker-Weg 6-10, 12165 Berlin, Germany

Email: huangb@zedat.fu-berlin.de

ABSTRACT

The East Asian summer monsoon (EASM) is an important part of the global climate system and plays a vital role in the Asian climate. Its sub-seasonal-to-seasonal predictability is a long-standing issue within the monsoon scientist community. In this study, we analyse the seasonal (with six months lead time) prediction skill of the EASM rainfall and its associated general circulation in non-initialised and initialised simulations for the years 1979-2005 performed by six prediction systems (*i.e.*, the BCC-CSM1-1, the CanCM4, the GFDL-CM2p1, the HadCM3, the MIROC5 and the MPI-ESM-LR) from the Coupled Model Intercomparison Project phase 5 (CMIP 5). We find that the simulation of the zonal wind is significantly improved in initialised simulations compared to non-initialised simulations. Based on the knowledge that zonal wind indices can be used as potential predictors for the EASM, we selected an EASM index based upon the zonal wind for further analysis. The assessment show that the GFDL-CM2p1 and the MIROC5 add prediction skill in simulating the EASM index with initialisation, the BCC-CSM1-1, the CanCM4, and the MPI-ESM-LR change the skill insignificantly, and the HadCM3 indicates a decreased skill score. The different response to the initialisation can be traced back to the ability of the models to capture the ENSO (El Niño-Southern Oscillation)-EASM coupled mode, particularly the Southern Oscillation-EASM coupled mode. As it is known from observational studies, this mode links the oceanic circulation and the EASM rainfall. In summary, we find that the GFDL-CM2p1 and the MIROC5 are capable to predict the EASM on a seasonal time-scale after initialisation.

Key Words: East Asian summer monsoon; initialisation; seasonal prediction; ENSO-EASM coupled mode; CMIP5

1. INTRODUCTION

The Asian monsoon is the most powerful monsoon system in the world due to the thermal contrast between the Eurasian continent and the Indo-Pacific Ocean. Its evolution and variability critically influences the livelihood and the socio-economic status of over two billion residents who live in the Asian monsoon dominated region. It encompasses two sub-monsoon systems (e.g., South Asian monsoon-SAM and East Asian monsoon-EAM; Wang, 2006). In summer time (June-July-August), the EAM, namely, the East Asian summer monsoon (EASM) occurs from the Indo-China peninsula to the Korean Peninsula and Japan, and shows strong intraseasonal-to-interdecadal variability (Ding and Chan, 2005). Thus, accurate predictions of the EASM is an important and long-standing issue in climate science.

To predict the EASM, there are two approaches, statistical prediction and dynamical prediction, respectively. The statistical method seeks the relationship between the EASM and a strong climate signal (e.g., ENSO, NAO; Wang et al., 2015;Wu et al., 2009;Yim et al., 2014). This method is limited by the strength of the climate signal. The other method is dynamical prediction. It employs climate model to predict the EASM (Kang and Yoo, 2006;Lee et al., 2010;Sperber et al., 2001;Wang et al., 2008a;Yang et al., 2008;Kim et al., 2012). Two kinds of climate models have been developed in the past few decades, atmosphere general circulation model (AGCM) and coupled atmosphere-ocean general circulation model (AOGCM). Both the two kinds of model have been used to predict the EASM (Kang et al., 2004;Wang et al., 2005;Wang et al., 2007;Wang et al., 2008a;Zhou et al., 2009). For AGCMs, the lower boundary conditions (*e.g.* SST: sea surface temperature) is required. An external ocean model is applied to predict the SST. Then the prescribed SST is employed as the lower boundary conditions to force the AGCMs. However, this method shows a low prediction skill over East Asia, especially in monsoon season (Wang et al., 2005;Barnston et al., 2010), because the AGCMs fail to produce the realistic SST-rainfall relationships in monsoon season (Wang et al., 2005;Wang et al., 2004). Therefore, the monsoon community endeavours to predict the EASM with AOGCMs (Zhou et al., 2009;Wang et al., 2008a;Jiang et al., 2013;Kim et al., 2012).

AOGCMs have proved to be the most valuable tools in predicting the EASM (Zhou et al., 2009;Wang et al., 2008a;Jiang et al., 2013;Kim et al., 2012). However, the performance of AOGCMs in predicting the EASM on seasonal time-scale strongly depends on their ability to reproduce the teleconnection between EASM and SST (Sperber et al., 2001) and the initialisation (Wang et al., 2005). In the coupled model inter-comparison project (CMIP)

phase 3 (CMIP3; Meehl et al., 2007) era, the models simulate not only a too weak SST-monsoon teleconnection (Kim et al., 2008;Kim et al., 2011), but also a too weak East Asian zonal wind-rainfall teleconnection (Sperber et al., 2013). Compared to CMIP3 models, CMIP phase 5 (CMIP5; Taylor et al., 2012) models improve the representation of monsoon status (Sperber et al., 2013). Therefore, given initial conditions, the CMIP5 models have potential to predict the EASM.

Initial conditions play a vital factor in predicting the EASM on sub-seasonal to seasonal time-scale (Kang and Shukla, 2006). Under current set up of initialisation, the CMIP5 models show the ability to predict the SST indicator (*i.e.*, El Niño-Southern Oscillation-ENSO index) up to 15 months in advance (Choi et al., 2016;Meehl et al., 2014;Meehl and Teng, 2012). This extended prediction skill of the ENSO suggests that the EASM can be predicted on a seasonal time-scale if the dynamic link between the ENSO and monsoon circulations is well represented in these models. Two scientific questions will be addressed in this study: 1. How realistic are the initialized CMIP5 models in representing the EASM? 2. To what extend reproduce the model's teleconnection between the ENSO and the EASM?

In this paper, we inter-compare the influence of the initialisation on the capability of the CMIP5 model to capture the EASM and the ENSO-EASM teleconnections. The model simulations, comparison data and methods are introduced in Section 2. Section 3 describes the seasonal skill of the rainfall predictions and the prediction of the associated general circulation of the EASM. The mechanism causing the differential response of the models to the initialisation is presented in Section 4. The discussions are shown in Section 5. Section 6 summaries the findings of this paper.

2. MODELS, DATA AND METHODS

2.1 MODELS AND INITIALISATION

In this study, we assess six prediction systems which have contributed to CMIP5 in historical and decadal hindcast simulations (Table 1). We employ these six prediction systems of CMIP5 in our study which have performed a yearly initialisation. Only these systems provide data to study the effect of initialisation on seasonal time-scale. The BCC-CSM1-1 has three ensemble members which are initialised on 1st September, 1st November and 1st January, respectively. The initialisation of HadCM3 takes place on each pre-year 1st November while the other four systems are initialised on 1st January. The full-field initialisation is named HadCM3-ff to distinguish it from the anomaly initialisation in HadCM3. Because of spatial

coverage of the precipitation observations, we select the satellite era (1979 to 2005) for our study. The first lead year results from initialised simulations are used to assess the seasonal predicting skills of the CMIP5 models. The initialisation strategies of all modelling groups from CMIP5 decadal prediction experiments have been summarised in Meehl *et al*. (2014). The brief configurations of the six prediction systems are presented in Table 2.

2.2 COMPARISON DATA

The main datasets which are used for the comparison in this study include: (1) monthly precipitation data from the Global Precipitation Climatology Project (GPCP; Adler et al., 2003); (2) monthly circulation data from ECMWF Interim re-analysis (ERA-Interim; Dee et al., 2011); and (3) monthly mean SST from National Oceanic and Atmospheric Administration (NOAA) improved Extended Reconstructed SST version 4 (ERSST v4; Huang et al., 2015). All the model data and the comparison data are remapped onto a common grid of 2.5ºx2.5º by bi-linear interpolation to reduce the uncertainty induced by different data resolutions.

2.3 METHODS

We apply the pattern correlation coefficient (PCC) to analyse the model performance in capturing the spatial pattern with reference to the observational data. It is the Pearson product-moment coefficient of linear correlation between a single variables on two different spatial patterns (Barnett and Schlesinger, 1987). There are two types of pattern correlation statistics: centred and un-centred. The centred (un-centred) statistic measures the similarity of two patterns after (without) the removal of the global mean. We choose the un-centred PCC in our study due to the fact that centred correlations alone are not sufficient for the attribution of seasonal prediction (Mitchell et al., 2001). The un-centred PCC is defined by:

$$PCC = \frac{\sum_{x=1}^{n}\sum_{y=1}^{m} w_{(x,y)} F_{(x,y)} A_{(x,y)}}{\sqrt{\sum_{x=1}^{n}\sum_{y=1}^{m} w_{(x,y)} F_{(x,y)}^{2} \sum_{x=1}^{n}\sum_{y=1}^{m} w_{(x,y)} A_{(x,y)}^{2}}}$$

where n and m are grids on longitude and latitude, respectively. $F_{(x,y)}$ and $A_{(x,y)}$ represent two dimensions comparison and validating value. $w_{(x,y)}$ indicates the weighting coefficient for each grid. An equal weighting coefficient was applied due to the study area is East Asia where we can omit the convergence of the longitudes with the latitudes

We also employ the anomaly correlation coefficient (ACC) to analyse the model performance in reproducing observational variations. The ACC is the correlation between

anomalies of forecasts and those of verifying values with the reference values, such as climatological values (Drosdowsky and Zhang, 2003). Its definition is:

$$ACC = \frac{\sum_{i=1}^{n} w_i (f_i - \bar{f})(a_i - \bar{a})}{\sqrt{\sum_{i=1}^{n} w_i (f_i - \bar{f})^2 \sum_{i=1}^{n} w_i (a_i - \bar{a})^2}}, (-1 \le ACC \le 1)$$

$$f_i = F_i - C_i, \bar{f} = \left(\sum_{i=1}^{n} w_i f_i \right) \Big/ \sum_{i=1}^{n} w_i$$

$$a_i = A_i - C_i, \bar{a} = \left(\sum_{i=1}^{n} w_i a_i \right) \Big/ \sum_{i=1}^{n} w_i$$

where n is the number of number of samples, and F_i, A_i, C_i represent comparison, verifying value, and reference value such as climatological value, respectively. Also, $\bar{f}$ is the mean of f_i, $\bar{a}$ is the mean of a_i, and w_i indicates the weighting coefficient. If the variation of anomalies of comparison dataset is perfectly coincident with that of the anomalies of verifying value, ACC will take 1 (the maximum value). Otherwise, if the variation is completely reversed, ACC is -1 (the minimum value).

The root-mean-square-error (RMSE) is employed to check the model deviation from the observation and its definition is:

$$RMSE = \sqrt{\sum_{i=1}^{n} w_i D_i^2} \Big/ \sqrt{\sum_{i=1}^{n} w_i}$$

where D_i represents the deviation between comparison and verifying value, w_i is the weighting coefficient for each sample, and n is the number of samples. If RMSE is closer to zero, it means that the comparisons are closer to the verifying values.

3. SEASONAL PREDICTION SKILL OF THE EASM

The EASM has complex spatial and temporal structures that encompass the tropics, subtropics, and midlatitudes (Tao and Chen, 1987;Ding, 1994). In late spring, an enhanced rainfall pattern is observed in the Indochina Peninsula and in South China Sea. Then, the rainfall belt advances northwards to the south of China. In early summer, the rainfall concentration occurs in the Yangtze River Basin and in southern Japan, namely, the Meiyu

and Baiu season, respectively. The rainfall belt can reach as far as northern China, the Korean Peninsula (called the Changma rainy season) and central Japan in July (Ding, 2004;Ding and Chan, 2005).

The EASM is characterised by both seasonal heterogeneous rainfall distribution and associated large-scale circulation systems (Wang et al., 2008b). In the summer season, water moisture migrates from the Pacific Ocean to central and eastern Asia, which is carried by the southwest surface winds. Generally, a strong summer monsoon year is followed by precipitation in northern China, while a weak summer monsoon year is usually accompanied by heavier rainfall along the Yangtze River basin (Zhou and Yu, 2005;Ding, 1994).

The prediction skill of the EASM rainfall and the associated general circulation variable (*i.e.*, zonal and meridional wind, and mean sea level pressure) is presented in Figure 1. These variables are resource of monsoon index (Wang et al., 2008b). Table 3 shows the contribution of these variables in the EASM. Their abbreviations follow the guideline of CMIP5 (Taylor et al., 2012). Without initialisation, the models show an acceptable performance in capturing the observed spatial variation (with high PCC) of the six variables, but a poor performance in simulating their temporal variation (with low ACC). After initialisation, we can see that the models show a higher ACC of the six variables. However, there is no improvement in simulating the spatial variation (PCC). The improvement of simulating the temporal variation of zonal winds (*i.e.*, ua850 and ua200) is larger than of the rainfall and meridional winds. One can exploit this improvement by using, a general circulation based monsoon index as a tool to predict the EASM.

In the recent decades, more than 25 general circulation indices have been produced to research the variability and long-term change of the EASM. Wang *et al.* (2008) classified them into five categories and discussed their ability to capture the main features of the EASM. They found that the Wang and Fan index (hereafter WF-index; 1999) shows the best performance in capturing the total variance of the precipitation and three-dimensional circulation over East Asia. We, thus, select the WF-index for the further analysis. Its definition is standardised average zonal wind at 850 hPa in (5°-15ºN, 90°-130ºE) minus in (22.5°-32.5ºN, 110°-140ºE). The WF-index is a shear vorticity index which often described by a north-south gradient of the zonal winds. In positive (negative) phase of the WF-index years, two strong (weak) rainfall belts locate at the Indo China Peninsula-to-the Philippine Sea and the northern China-to-the Japan Sea, and a weak (strong) rainfall belt occurs from the Yangtze river basin-to-the south of Japan.

In the non-initialised simulations, none of the models captures the observed EASM, as indicated by an insignificant ACC (Figure 2). The CanCM4 and the GFDL-CM2p1 simulate a negative phase, while the BCC-CSM1-1, the HadCM3, the MIROC5 and the MPI-ESM-LR all predict a positive phase of the EASM. After initialisation, the CanCM4, the GFDL-CM2p1 and the MIROC5 improve the skill to simulate the EASM, the MPI-ESM-LR displays hardly any reaction, while the BCC-CSM1-1 and the HadCM3 shows a worse performance than before. Particularly with anomaly initialisation, the HadCM3 significantly loses its prediction skill in capturing the EASM. The CMIP5 models show different response to the initialisation in predicting the EASM on seasonal time-scale. To understand the potential reason, we analysis the principle components of six variables which contribute to the EASM. The details are presented in Section 4.

4. EASM-ENSO COUPLED MODE IN CMIP5

We employ the EOF method to analyse the leading EOF modes of six meteorological variables anomaly in the EASM region (0°-50ºN, 100°-140ºE). The first EOF mode of rainfall is characterised by a "sandwich" pattern which shows sharp contrast between the prominent rainfall centre over Malaysia, the Yangtze River valley and the south of Japan, and the enhanced rainfall over the Indo-China Peninsula and the Philippine Sea. The increased precipitation is associated with cyclones in the low-level (850 hPa) and anti-cyclones in the upper level (200 hPa) (not shown).

The correlation coefficient of the first eigenvector and the associated principal component (PC) between the model simulation and the observation in the non-initialised and the initialised simulation is presented in Figure 3. The models can capture the eigenvector of the first EOF for the six meteorological fields in non-initialised simulation. However, they fail to reproduce the associated PC of the first leading EOF mode. Compared to the non-initialised simulation, the models show no improvement to simulate the first leading EOF mode of rainfall, but exhibit a better performance in representing the first leading EOF mode of zonal wind. The CanCM4 and the GFDL-CM2p1 capture the first PC of ua850, but not the other five models. For the zonal wind at 200 hPa, the BCC-CSM1-1 fails to simulate its first EOF mode while the other six models can. Then, only the GFDL-CM2p1 accurately simulates the first EOF eigenvectors and the associated PC of va850, which cannot be reproduced in the other models. None of the models captures the spatial-temporal variation of the first EOF mode of meridional wind at 200 hPa. In addition, the GFDL-CM2p1 and the

MIROC5 simulates a reasonable leading EOF mode and associated PC of psl, while the other models do not capture it.

Figure 4 shows the fractional (percentage) variances of the six variables of the first EOF mode with the total variances from the observation, and the model simulation in non-initialisation and in initialisation. The observational total variances for the pr, the ua850, the ua200, the va850, the va200 and the psl, are depicted by the first lead EOF mode in 21.2, 59.0, 36.5, 20.6, 28.5 and 50.0 percent, respectively. The models simulate the comparable explanatory variances, which show a slight discrepancy for the first leading mode in the non-initialisation. From non-initialised simulation to initialised simulation, the CGCMs tend to enhance the first EOF lead mode due to the fact that they show larger fractional variances of the total variances of the six variables. We note that the CanCM4 and the GFDL-CM2p1 significantly increase the fractional variances from non-initialisation to initialisation.

The ENSO is a dominant mode of the inter-annual variability of the coupled ocean and atmosphere climate system, which has strong effects on the inter-annual variation of the EASM (Wu et al., 2003;Wang et al., 2000). Wang et al. (2015) summarised the first EOF lead mode of the ASM is the ENSO developing mode. As previously mentioned, the first EOF mode is improved in the initialised simulations, compared to the non-initialised simulation. This also can be found in the ENSO indices (Figure 5). Niño3.4 is calculated by the SST anomaly in the central Pacific (190-240ºE, 5ºS-5ºN), while the southern oscillation index (SOI) is based upon the anomaly of the sea level pressure differences between Tahiti (210.75ºE, 17.6ºS) and Darwin (130.83ºE, 12.5ºS). To calculate the SOI, we interpolate the grid data to the Tahiti and the Darwin point by bilinear interpolation.

The individual members and their ensemble mean of the six models show a low correlation coefficient to the observational Niño3.4 and the SOI in the non-initialised simulations. Niño3.4 and SOI represent the oscillation of two components in the earth system, the ocean and the atmosphere, respectively. These two indices show strong anti-phase in the observation, with correlation range is -0.94 to -0.92 for four seasons (DJF, MAM, JJA, SON; Figure 5). The models describe the anti-correlation between Niño3.4 and the SOI, but weaker than observed. Compared to the non-initialisation, there is a significant improvement for models in capturing the observational Niño3.4 and the SOI after initialisation. Initialisation lowers the spread of ensemble members in predicting Niño3.4 and the SOI in all the six models. However, initialisation does not prominently change the correlation between Niño3.4 and the SOI in the model simulations. With initialisation, the

GFDL model shows a weaker correlation between Niño3.4 and the SOI, while the HadCM3 models illustrate a stronger correlation. It is worth mentioning that after initialisation the ensemble mean of each model outperforms its individual members in capturing Niño3.4 and the SOI. The correlation coefficient between Niño3.4 and the SOI of MME is ~0.8 in both non-initialised and initialised simulations.

The EASM strongly relies on the pre-seasons ENSO signal due to the lag response of the atmosphere to the SST anomaly (Wu et al., 2003). The lead-lag correlation coefficients between the EASM index and the Niño3.4, and the SOI from JJA(-1) to JJA(+1) are illustrated in Figure 6. The pre-season Niño3.4 (SOI) presents a significant negative (positive) correlation to the EASM, while the post-season Niño3.4 (SOI) shows a notable positive (negative) correlation. This lead-lag correlation coefficient phase is called the Niño3.4-/SOI-EASM coupled mode (Wang et al., 2008b). In the non-initialised cases, the models do not produce the teleconnection between the ENSO and the EASM. The CanCM4, the HadCM3 and the MPI-ESM-LR fail to represent the lead-lag correlation coefficient difference between pre-/post-season ENSO and EASM. The BCC-CSM1-1, the GFDL-CM2p1 and the MIROC5 capture the coupled mode of the ENSO and the EASM. However, the pre-season ENSO has a weak effect on the EASM. Compared to the non-initialised cases, the MIROC5 and the GFDL-CM2p1 both demonstrate a significant improvement in simulating Niño3.4 (SOI)-EASM coupled mode in the initialisation. The BCC-CSM1-1, the HadCM3, and the HadCM3-ff show no improvement, with insignificant correlation between Niño3.4 (SOI) and the EASM. The CanCM4 and the MPI-ESM-LR indicate a higher correlation between the EASM and the simultaneous-to-post-season ENSO than to the pre-season ENSO.

5. DISCUSSION

The model exhibits a better performance in simulating the general circulation of the EASM with initialisation. Thus, initialisation is helpful in forecasting the EASM on a seasonal time-scale. There are two initialisation methods in our study, full-field initialisation and anomaly initialisation (Table 1). The full-field initialisation produces more skilful predictions on the seasonal time-scale in predicting regional temperature and precipitation (Magnusson et al., 2013;Smith et al., 2013). But, for predicting the EASM, there is no significant difference between the two methods. We can see that both the GFDL-CM2p1 and the MIROC5 have a significant improvement in capturing the EASM, with full-field and anomaly initialisation, respectively. Only the HadCM3 was initialised by the two

initialisation techniques. However, both these two initialised techniques are producing poor predictions of the EASM with no major differences.

The initialisation strategy of the models is to initialise with the observed atmospheric component (*i.e.*, zonal and meridional wind, geopotential height, *etc*.) and the SST (Meehl et al., 2009;Meehl et al., 2014;Taylor et al., 2012). With initialisation, the SST conveys its information via the large heat content of ocean to the coupled system. Therefore, an index indicating an ocean oscillation like Niño3.4 shows a seasonal-to-decadal prediction skill (Choi et al., 2016;Luo et al., 2008;Jin et al., 2008). The models studied here demonstrate a prediction skill in simulating Niño3.4 and the SOI due to this effect. The change of the correlation between Niño3.4 and the SOI is insignificant from non-initialised to initialised simulations. We therefore conclude that the relationship between Niño3.4 and the SOI depends more on the model parameterisation than on the initial condition.

Wang *et al*. (2015) found that the second EOF mode of ASM is the Indo-western Pacific monsoon-ocean coupled mode, the third is the Indian Ocean dipole (IOD) mode, and the fourth is trend mode. The Indo-western Pacific monsoon-ocean coupled mode is the atmosphere-ocean interaction mode (Xiang et al., 2013;Wang et al., 2013), which is supported by positive thermodynamic feedback between the western North Pacific (WNP) anticyclone and the underlying Indo-Pacific sea surface temperature anomaly dipole over the warm pool (Wang et al., 2015). The IOD increases the precipitation from the South Asian subcontinent to south-eastern China and suppresses the precipitation over the WNP (Wang et al., 2015). It affects the Asian monsoon by the meridional asymmetry of the monsoonal easterly shear during the boreal summer, which can particularly strengthen the northern branch of the Rossby wave response to the south-eastern Indian Ocean SST cooling, leading to an intensified monsoon flow as well as an intensified convection (Wang and Xie, 1996;Wang et al., 2003;Xiang et al., 2011;Wang et al., 2015). We noted that the models simulate a reasonable first EOF mode (Figure 3), but illustrate no skill in capturing the other EOF leading modes (not shown). We argue that the models cannot well represent the monsoon-ocean interaction, even with initialisation. Then, the models do not simulate the third EOF leading mode of the EASM since the predictability of the IOD extends only over a three-month time-scale (Choudhury et al., 2015). The current initialisation strategies (both anomaly and full-field) enhance the ENSO signal in the model simulations with higher explained fraction of variance. Kim et al. (2012) described a similar finding in ECMWF System 4 and NCEP Climate Forecast System version 2 (CFSv2) seasonal prediction

simulations. This overly strong modulation of the EASM by ENSO due to the models well predict ENSO on seasonal time-scale with initialisation (Kim et al., 2012;Jin et al., 2008).

It is worth mentioning that it was an extremely weak monsoon and strong El Niño year in 1998. The CanCM4, the GFDL-CM2p1, the MIROC5 and the MPI-ESM-LR have the ability to simulate the extreme monsoon event, while the BCC-CSM1-1, and the HadCM3 do not capture it even with initialisation. There is potential for the BCC-CSM and the HadCM models to improve the teleconnection between the ENSO and the EASM.

This study has discussed six CMIP5 models in predicting the EASM on seasonal time-scale. The six models are earth system coupled models which present a better SST-monsoon teleconnection than IRI (International Research Institute for Climate and Society) models (Barnston et al., 2010) and CMIP3 models (Sperber et al., 2013). The CMIP5 models show a comparable prediction skill as current seasonal forecast application systems, the ECMWF System and the NCEP CFS, respectively. Both the two application systems have low prediction skill of EASM (Jiang et al., 2013;Kim et al., 2012).

We have compared six CMIP5 systems with their respective initialisation strategies. The GFDL-CM2p1 and the MIROC5 have the potential to serve as seasonal forecast application system even with their current initialisation method. These models have great potential to optimise the SST-EASM interaction simulation performance to improve their seasonal prediction skill of the EASM.

6. SUMMARY

Six earth system models from CMIP5 have been selected in our study. We have analysed the improvement of the rainfall, the mean sea level pressure, the zonal wind and the meridional wind in the EASM region from non-initialisation to initialisation. The low prediction skill of the summer monsoon precipitation is due to the uncertainties of cloud physics and cumulus parameterisations in the models (Lee et al., 2010;Seo et al., 2015). The models show a better performance in capturing the inter-annual variability of zonal wind than the precipitation after initialisation (Figure 1). Thus, the zonal wind index is an additional factor which can indicate the prediction skill of the model. When, we calculate the WF-index in both non-initialised and initialised simulations, the GFDL-CM2p1 and the MIROC5 show a significant advancement in simulating the EASM from non-initialised to initialised simulation with a lower RMSE and a higher ACC (Figure 2). There is only a slight change in the WF-index calculated from the BCC-CSM1-1, the CanCM4 and the MPI-ESM-LR data after

initialisation. Compared to the non-initialised simulation, the HadCM3 loses prediction skill, especially with anomaly initialisation.

To test the possible mechanisms of the models' performance in the non-initialisation and the initialisation, we have calculated the leading mode of the six fields which are associated to the EASM. The models demonstrate a better agreement with the observational first EOF mode in the initialised simulations (Figure 3). The first lead mode of zonal wind at 200 hPa shows a significant improvement in the models except the BCC-CSM1-1 with initialisation. Therefore, a potential predictor might be an index based upon the zonal wind at 200 hPa. Compared to the non-initialisation, the models enhance the first EOF mode with a higher fraction of variance to the total variance after initialisation (Figure 4). The first EOF mode of the EASM is the ENSO developing mode (Wang et al., 2015). We have analysed the seasonal simulating skill of Niño3.4 and the SOI in each model (Figure 5). The models show a poor performance in representing Niño3.4 and the SOI in the non-initialised simulation. Initialisation improves the model simulating skill of Niño3.4 and the SOI. The initialised simulations decrease the spread of ensemble members in the models. We found that there is no significant change in the models reproducing the correlation between Niño3.4 and the SOI from non-initialisation to initialisation.

In general, the pre-season warm phase of the ENSO (El Niño) leads to a weak EASM producing more rainfall over the South China Sea and northwest China, and less rainfall over the Yangtze River Valley and the southern Japan; the cold phase of the ENSO (La Niña) illustrates a reverse rainfall pattern to El Niño in East Asia. The pre-season Niño3.4 (SOI) exhibits a strong negative (positive) correlation to the EASM, while the correlation between the post-season Niño3.4 (SOI) and the EASM illustrates an anti-phase as the pre-season (Figure 6). In the non-initialised simulations, the models do not capture Niño3.4-/SOI-EASM coupled mode. We found that only the MIROC5 has the ability to represent the Niño3.4-EASM coupled mode with initialisation. For the SOI-EASM coupled mode, the GFDL-CM2p1 and the MIROC5 capture it in the initialisation, while the BCC-CSM1-1, the HadCM3, the HadCM2-ff, the CanCM4 and the MPI-ESM-LR do not. Therefore, we argue that the differential response to the initialisation in the CMIP5 models due to their differential depiction of ENSO-EASM coupled mode.

Acknowledgements

This work was supported by the China Scholarship Council (CSC) and the Freie Universität Berlin. We would like to thank the climate modelling groups listed in Table 1 of this paper

for producing and making their model output available. We acknowledge the MiKlip project funded by the Federal Ministry of Education and Research and the German Climate Computing Centre (DKRZ) for providing the data services.

References

Adler, R. F., Huffman, G. J., Chang, A., Ferraro, R., Xie, P.-P., Janowiak, J., Rudolf, B., Schneider, U., Curtis, S., Bolvin, D., Gruber, A., Susskind, J., Arkin, P., and Nelkin, E.: The Version-2 Global Precipitation Climatology Project (GPCP) Monthly Precipitation Analysis (1979–Present), J Hydrometeorol, 4, 1147-1167, 10.1175/1525-7541(2003)004<1147:tvgpcp>2.0.co;2, 2003.

Arora, V. K., Scinocca, J. F., Boer, G. J., Christian, J. R., Denman, K. L., Flato, G. M., Kharin, V. V., Lee, W. G., and Merryfield, W. J.: Carbon emission limits required to satisfy future representative concentration pathways of greenhouse gases, Geophys Res Lett, 38, L05805, 10.1029/2010gl046270, 2011.

Barnett, T. P., and Schlesinger, M. E.: Detecting Changes in Global Climate Induced by Greenhouse Gases, J Geophys Res Atmos, 92, 14772-14780, 10.1029/JD092iD12p14772, 1987.

Barnston, A. G., Li, S. H., Mason, S. J., DeWitt, D. G., Goddard, L., and Gong, X. F.: Verification of the First 11 Years of IRI's Seasonal Climate Forecasts, J Appl Meteorol Clim, 49, 493-520, 10.1175/2009jamc2325.1, 2010.

Choi, J., Son, S. W., Ham, Y. G., Lee, J. Y., and Kim, H. M.: Seasonal-to-Interannual Prediction Skills of Near-Surface Air Temperature in the CMIP5 Decadal Hindcast Experiments, J Clim, 29, 1511-1527, 10.1175/Jcli-D-15-0182.1, 2016.

Choudhury, D., Sharma, A., Sivakumar, B., Sen Gupta, A., and Mehrotra, R.: On the predictability of SSTA indices from CMIP5 decadal experiments, Environ Res Lett, 10, 074013, 10.1088/1748-9326/10/7/074013, 2015.

Dee, D. P., Uppala, S. M., Simmons, A. J., Berrisford, P., Poli, P., Kobayashi, S., Andrae, U., Balmaseda, M. A., Balsamo, G., Bauer, P., Bechtold, P., Beljaars, A. C. M., van de Berg, L., Bidlot, J., Bormann, N., Delsol, C., Dragani, R., Fuentes, M., Geer, A. J., Haimberger, L., Healy, S. B., Hersbach, H., Holm, E. V., Isaksen, L., Kallberg, P., Kohler, M., Matricardi, M., McNally, A. P., Monge-Sanz, B. M., Morcrette, J. J., Park, B. K., Peubey, C., de Rosnay, P., Tavolato, C., Thepaut, J. N., and Vitart, F.: The ERA-Interim reanalysis: configuration and performance of the data assimilation system, Q J R Meteorolog Soc, 137, 553-597, 10.1002/qj.828, 2011.

Delworth, T. L., Broccoli, A. J., Rosati, A., Stouffer, R. J., Balaji, V., Beesley, J. A., Cooke, W. F., Dixon, K. W., Dunne, J., Dunne, K. A., Durachta, J. W., Findell, K. L., Ginoux, P., Gnanadesikan, A., Gordon, C. T., Griffies, S. M., Gudgel, R., Harrison, M. J., Held, I. M., Hemler, R. S., Horowitz, L. W., Klein, S. A., Knutson, T. R., Kushner, P. J., Langenhorst, A. R., Lee, H. C., Lin, S. J., Lu, J., Malyshev, S. L., Milly, P. C. D., Ramaswamy, V., Russell, J., Schwarzkopf, M. D., Shevliakova, E., Sirutis, J. J., Spelman, M. J., Stern, W. F., Winton, M., Wittenberg, A. T., Wyman, B., Zeng, F., and Zhang, R.: GFDL's CM2 global coupled climate models. Part I: Formulation and simulation characteristics, J Clim, 19, 643-674, 10.1175/Jcli3629.1, 2006.

Ding, Y.: Seasonal march of the East-Asian summer monsoon., in: East Asian Monsoon, edited by: Chang, C.-P., World Scientific, Singapore, 560, 2004.

Ding, Y. H.: Monsoons over China, Kluwer Academic Publisher, Dordrecht/Boston/London, 419 pp., 1994.

Ding, Y. H., and Chan, J. C. L.: The East Asian summer monsoon: an overview, Meteorol Atmos Phys, 89, 117-142, 10.1007/s00703-005-0125-z, 2005.

426 Drosdowsky, W., and Zhang, H.: Verification of Spatial Fields, in: Forecast Verification: A
427 Practitioner's Guide in Atmospheric Science edited by: Jolliffe, L. T., and Stephenson, D. B.,
428 John Wiley & Sons Ltd, England, 128-129, 2003.
429 Huang, B. Y., Banzon, V. F., Freeman, E., Lawrimore, J., Liu, W., Peterson, T. C., Smith, T.
430 M., Thorne, P. W., Woodruff, S. D., and Zhang, H. M.: Extended Reconstructed Sea Surface
431 Temperature Version 4 (ERSST.v4). Part I: Upgrades and Intercomparisons, J Clim, 28, 911-
432 930, 10.1175/Jcli-D-14-00006.1, 2015.
433 Jiang, X. W., Yang, S., Li, Y. Q., Kumar, A., Liu, X. W., Zuo, Z. Y., and Jha, B.: Seasonal-
434 to-Interannual Prediction of the Asian Summer Monsoon in the NCEP Climate Forecast
435 System Version 2, J Clim, 26, 3708-3727, 10.1175/Jcli-D-12-00437.1, 2013.
436 Jin, E. K., Kinter, J. L., Wang, B., Park, C. K., Kang, I. S., Kirtman, B. P., Kug, J. S., Kumar,
437 A., Luo, J. J., Schemm, J., Shukla, J., and Yamagata, T.: Current status of ENSO prediction
438 skill in coupled ocean–atmosphere models, Clim Dyn, 31, 647-664, 10.1007/s00382-008-
439 0397-3, 2008.
440 Kang, I.-S., and Shukla, J.: Dynamic seasonal prediction and predictability of the monsoon,
441 in: The Asian Monsoon, edited by: Wang, B., Springer Berlin Heidelberg, Berlin, Heidelberg,
442 585-612, 2006.
443 Kang, I. S., Lee, J. Y., and Park, C. K.: Potential predictability of summer mean precipitation
444 in a dynamical seasonal prediction system with systematic error correction, J Clim, 17, 834-
445 844, 10.1175/1520-0442(2004)017<0834:Pposmp>2.0.Co;2, 2004.
446 Kang, I. S., and Yoo, J. H.: Examination of multi-model ensemble seasonal prediction
447 methods using a simple climate system, Clim Dyn, 26, 285-294, 10.1007/s00382-005-0074-8,
448 2006.
449 Kim, H. J., Wang, B., and Ding, Q. H.: The Global Monsoon Variability Simulated by
450 CMIP3 Coupled Climate Models, J Clim, 21, 5271-5294, 10.1175/2008jcli2041.1, 2008.
451 Kim, H. J., Takata, K., Wang, B., Watanabe, M., Kimoto, M., Yokohata, T., and Yasunari, T.:
452 Global Monsoon, El Nino, and Their Interannual Linkage Simulated by MIROC5 and the
453 CMIP3 CGCMs, J Clim, 24, 5604-5618, 10.1175/2011jcli4132.1, 2011.
454 Kim, H. M., Webster, P. J., Curry, J. A., and Toma, V. E.: Asian summer monsoon prediction
455 in ECMWF System 4 and NCEP CFSv2 retrospective seasonal forecasts, Clim Dyn, 39,
456 2975-2991, 10.1007/s00382-012-1470-5, 2012.
457 Lee, J.-Y., Wang, B., Kang, I. S., Shukla, J., Kumar, A., Kug, J. S., Schemm, J. K. E., Luo, J.
458 J., Yamagata, T., Fu, X., Alves, O., Stern, B., Rosati, T., and Park, C. K.: How are seasonal
459 prediction skills related to models' performance on mean state and annual cycle?, Clim Dyn,
460 35, 267-283, 10.1007/s00382-010-0857-4, 2010.
461 Luo, J.-J., Masson, S., Behera, S. K., and Yamagata, T.: Extended ENSO Predictions Using a
462 Fully Coupled Ocean–Atmosphere Model, J Clim, 21, 84-93, 10.1175/2007jcli1412.1, 2008.
463 Magnusson, L., Alonso-Balmaseda, M., Corti, S., Molteni, F., and Stockdale, T.: Evaluation
464 of forecast strategies for seasonal and decadal forecasts in presence of systematic model
465 errors, Clim Dyn, 41, 2393-2409, 10.1007/s00382-012-1599-2, 2013.
466 Matei, D., Pohlmann, H., Jungclaus, J., Muller, W., Haak, H., and Marotzke, J.: Two Tales of
467 Initializing Decadal Climate Prediction Experiments with the ECHAM5/MPI-OM Model, J
468 Clim, 25, 8502-8523, 10.1175/Jcli-D-11-00633.1, 2012.
469 Meehl, G., Covey, C., Delworth, T., Latif, M., McAvaney, B., Mitchell, J., Stouffer, R., and
470 Taylor, K.: The WCRP CMIP3 multi-model dataset: a new era in climate change research,
471 Bull Am Meteorol Soc, 88, 1383-1394, 2007.
472 Meehl, G. A., Goddard, L., Murphy, J., Stouffer, R. J., Boer, G., Danabasoglu, G., Dixon, K.,
473 Giorgetta, M. A., Greene, A. M., Hawkins, E., Hegerl, G., Karoly, D., Keenlyside, N.,
474 Kimoto, M., Kirtman, B., Navarra, A., Pulwarty, R., Smith, D., Stammer, D., and Stockdale,

T.: DECADAL PREDICTION Can It Be Skillful?, Bull Am Meteorol Soc, 90, 1467-1485, 10.1175/2009bams2778.1, 2009.
Meehl, G. A., and Teng, H. Y.: Case studies for initialized decadal hindcasts and predictions for the Pacific region, Geophys Res Lett, 39, L22705, 10.1029/2012gl053423, 2012.
Meehl, G. A., Goddard, L., Boer, G., Burgman, R., Branstator, G., Cassou, C., Corti, S., Danabasoglu, G., Doblas-Reyes, F., Hawkins, E., Karspeck, A., Kimoto, M., Kumar, A., Matei, D., Mignot, J., Msadek, R., Navarra, A., Pohlmann, H., Rienecker, M., Rosati, T., Schneider, E., Smith, D., Sutton, R., Teng, H. Y., van Oldenborgh, G. J., Vecchi, G., and Yeager, S.: DECADAL CLIMATE PREDICTION An Update from the Trenches, Bull Am Meteorol Soc, 95, 243-267, 10.1175/Bams-D-12-00241.1, 2014.
Mitchell, J. F. B., Karoly, D. J., Hegerl, G. C., Zwiers, F. W., Allen, M. R., and Marengo, J.: Detection of Climate Change and Attribution of Causes, in: Third Assessment Report of the Intergovernmental Panel on Climate Change., edited by: Houghton, J. T., Griggs, D. J., Noguer, M., van der Linden, P. J., Dai, X., Maskell, K., and Johnson, C. A., Cambridge University Press, New York, 470, 2001.
Seo, K. H., Son, J. H., Lee, J. Y., and Park, H. S.: Northern East Asian Monsoon Precipitation Revealed by Airmass Variability and Its Prediction, J Clim, 28, 6221-6233, 10.1175/Jcli-D-14-00526.1, 2015.
Smith, D. M., Eade, R., and Pohlmann, H.: A comparison of full-field and anomaly initialization for seasonal to decadal climate prediction, Clim Dyn, 41, 3325-3338, 10.1007/s00382-013-1683-2, 2013.
Sperber, K., Annamalai, H., Kang, I. S., Kitoh, A., Moise, A., Turner, A., Wang, B., and Zhou, T.: The Asian summer monsoon: an intercomparison of CMIP5 vs. CMIP3 simulations of the late 20th century, Clim Dyn, 41, 2711-2744, 10.1007/s00382-012-1607-6, 2013.
Sperber, K. R., Brankovic, C., Deque, M., Frederiksen, C. S., Graham, R., Kitoh, A., Kobayashi, C., Palmer, T., Puri, K., Tennant, W., and Volodin, E.: Dynamical seasonal predictability of the Asian summer monsoon, Mon Weather Rev, 129, 2226-2248, 10.1175/1520-0493(2001)129<2226:Dspota>2.0.Co;2, 2001.
Tao, S. Y., and Chen, L. X.: A review of recent research on the East Asian summer monsoon in China, in: Monsoon Meterology, edited by: Chang, C.-P., and Krishnamurti, T. N., Oxford University Press, Oxford, 60-92, 1987.
Tatebe, H., Ishii, M., Mochizuki, T., Chikamoto, Y., Sakamoto, T. T., Komuro, Y., Mori, M., Yasunaka, S., Watanabe, M., Ogochi, K., Suzuki, T., Nishimura, T., and Kimoto, M.: The Initialization of the MIROC Climate Models with Hydrographic Data Assimilation for Decadal Prediction, J Meteorol Soc Japan, 90a, 275-294, 10.2151/jmsj.2012-A14, 2012.
Taylor, K. E., Stouffer, R. J., and Meehl, G. A.: An Overview of Cmip5 and the Experiment Design, Bull Am Meteorol Soc, 93, 485-498, 10.1175/Bams-D-11-00094.1, 2012.
Wang, B., and Xie, X.: Low-Frequency Equatorial Waves in Vertically Sheared Zonal Flow. Part I: Stable Waves, J Atmos Sci, 53, 449-467, 10.1175/1520-0469(1996)053<0449:lfewiv>2.0.co;2, 1996.
Wang, B., and Fan, Z.: Choice of south Asian summer monsoon indices, Bull Am Meteorol Soc, 80, 629-638, 10.1175/1520-0477(1999)080<0629:Cosasm>2.0.Co;2, 1999.
Wang, B., Wu, R. G., and Fu, X. H.: Pacific-East Asian teleconnection: how does ENSO affect East Asian climate?, J Clim, 13, 1517-1536, 2000.
Wang, B., Wu, R., and Li, T.: Atmosphere–Warm Ocean Interaction and Its Impacts on Asian–Australian Monsoon Variation*, J Clim, 16, 1195-1211, 10.1175/1520-0442(2003)16<1195:aoiaii>2.0.co;2, 2003.
Wang, B., Kang, I.-S., and Lee, J.-Y.: Ensemble Simulations of Asian–Australian Monsoon Variability by 11 AGCMs*, J Clim, 17, 803-818, 10.1175/1520-0442(2004)017<0803:esoamv>2.0.co;2, 2004.

Wang, B., Ding, Q. H., Fu, X. H., Kang, I. S., Jin, K., Shukla, J., and Doblas-Reyes, F.: Fundamental challenge in simulation and prediction of summer monsoon rainfall, Geophys Res Lett, 32, L15711, 10.1029/2005gl022734, 2005.
Wang, B.: The Asian Monsoon, Springer Science & Business Media, Praxis, New York, NY, USA, 2006.
Wang, B., Lee, J.-Y., Kang, I. S., Shukla, J., Kug, J. S., Kumar, A., Schemm, J., Luo, J. J., Yamagata, T., and Park, C. K.: How accurately do coupled climate models predict the leading modes of Asian-Australian monsoon interannual variability?, Clim Dyn, 30, 605-619, 10.1007/s00382-007-0310-5, 2007.
Wang, B., Lee, J.-Y., Kang, I.-S., Shukla, J., Park, C. K., Kumar, A., Schemm, J., Cocke, S., Kug, J. S., Luo, J. J., Zhou, T., Wang, B., Fu, X., Yun, W. T., Alves, O., Jin, E. K., Kinter, J., Kirtman, B., Krishnamurti, T., Lau, N. C., Lau, W., Liu, P., Pegion, P., Rosati, T., Schubert, S., Stern, W., Suarez, M., and Yamagata, T.: Advance and prospectus of seasonal prediction: assessment of the APCC/CliPAS 14-model ensemble retrospective seasonal prediction (1980–2004), Clim Dyn, 33, 93-117, 10.1007/s00382-008-0460-0, 2008a.
Wang, B., Wu, Z. W., Li, J. P., Liu, J., Chang, C. P., Ding, Y. H., and Wu, G. X.: How to measure the strength of the East Asian summer monsoon, J Clim, 21, 4449-4463, 10.1175/2008jcli2183.1, 2008b.
Wang, B., Xiang, B., and Lee, J. Y.: Subtropical high predictability establishes a promising way for monsoon and tropical storm predictions, Proc Natl Acad Sci U S A, 110, 2718-2722, 10.1073/pnas.1214626110, 2013.
Wang, B., Lee, J. Y., and Xiang, B. Q.: Asian summer monsoon rainfall predictability: a predictable mode analysis, Clim Dyn, 44, 61-74, 10.1007/s00382-014-2218-1, 2015.
Wu, R. G., Hu, Z. Z., and Kirtman, B. P.: Evolution of ENSO-related rainfall anomalies in East Asia, J Clim, 16, 3742-3758, 10.1175/1520-0442(2003)016<3742:Eoerai>2.0.Co;2, 2003.
Wu, T. W., Song, L. C., Li, W. P., Wang, Z. Z., Zhang, H., Xin, X. G., Zhang, Y. W., Zhang, L., Li, J. L., Wu, F. H., Liu, Y. M., Zhang, F., Shi, X. L., Chu, M., Zhang, J., Fang, Y. J., Wang, F., Lu, Y. X., Liu, X. W., Wei, M., Liu, Q. X., Zhou, W. Y., Dong, M., Zhao, Q. G., Ji, J. J., Li, L., and Zhou, M. Y.: An Overview of BCC Climate System Model Development and Application for Climate Change Studies, J Meteorol Res-Prc, 28, 34-56, 10.1007/s13351-014-3041-7, 2014.
Wu, Z. W., Wang, B., Li, J. P., and Jin, F. F.: An empirical seasonal prediction model of the east Asian summer monsoon using ENSO and NAO, J Geophys Res Atmos, 114, D18120, 10.1029/2009jd011733, 2009.
Xiang, B., Wang, B., Yu, W., and Xu, S.: How can anomalous western North Pacific Subtropical High intensify in late summer?, Geophys Res Lett, 40, 2349-2354, 10.1002/grl.50431, 2013.
Xiang, B. Q., Yu, W. D., Li, T., and Wang, B.: The critical role of the boreal summer mean state in the development of the IOD, Geophys Res Lett, 38, L02710, 10.1029/2010gl045851, 2011.
Yang, S., Zhang, Z. Q., Kousky, V. E., Higgins, R. W., Yoo, S. H., Liang, J. Y., and Fan, Y.: Simulations and seasonal prediction of the Asian summer monsoon in the NCEP Climate Forecast System, J Clim, 21, 3755-3775, 10.1175/2008jcli1961.1, 2008.
Yim, S. Y., Wang, B., and Xing, W.: Prediction of early summer rainfall over South China by a physical-empirical model, Clim Dyn, 43, 1883-1891, 10.1007/s00382-013-2014-3, 2014.
Zhou, T., Wu, B., and Wang, B.: How Well Do Atmospheric General Circulation Models Capture the Leading Modes of the Interannual Variability of the Asian–Australian Monsoon?, J Clim, 22, 1159-1173, 10.1175/2008jcli2245.1, 2009.

574 Zhou, T. J., and Yu, R. C.: Atmospheric water vapor transport associated with typical
575 anomalous summer rainfall patterns in China, J Geophys Res Atmos, 110, D08104,
576 10.1029/2004jd005413, 2005.

577

578 Table 1. Details of the prediction systems investigated in this study.

System	Institute	Resolution		Non-Initialisation	Initialisation		Reference
		Atmospheric	Oceanic	Members	Members	Type	
BCC-CSM1-1	Beijing Climate Center, China	T42L26	1lonx1.33lat L40	3	3	Full-field	Wu *et al*. (2014)
CanCM4	Canadian Centre for Climate Modelling and Analysis, Canada	T63L35	256 x 192 L40	10	10	Full-field	Arora *et al*. (2011)
GFDL-CM2p1	Geophysical Fluid Dynamics Laboratory, USA	N45L24	1lon x 0.33-1lat L50	10	10	Full-field	Delworth *et al*. (2006)
HadCM3	Met Office Hadley Centre, UK	N48L19	1.25x1.25 L20	10	10 + 10	Full-field and Anomaly	Smith *et al*. (2013)
MIROC5	Atmosphere and Ocean Research Institute, Japan	T85L40	256x192 L44	5	6	Anomaly	Tatebe *et al*. (2012)
MPI-ESM-LR	Max Planck Institute for Meteorology, Germany	T63L47	GR15 L40	3	3	Anomaly	Matei *et al*. (2012)

579

Table 2. Brief summaries of initialisation strategies used by modelling groups in the study. ECMWF: European Centre for Medium-Range Weather Forecasts; GODAS: Global Ocean Data Assimilation System; NCEP: National Centers for Environmental Prediction; S: Salinity; SODA: Simple Ocean Data Assimilation; T: Temperature.

system	Atmosphere	Ocean	Internet
BCC-CSM1-1	-	integration with ocean T nudged to SODA product above 1500 m	http://forecast.bcccsm.ncc-cma.net/
CanCM4	ECMWF re-analysis	off-line assimilation of SODA and GODAS subsurface ocean T and S adjusted to reserve model T-S	http://www.cccma.ec.gc.ca/
GFDL-CM2p1	GFDL re-analysis	assimilates observations of T, S from World Ocean Database	https://www.gfdl.noaa.gov/multidecadal-prediction-stream/
HadCM3	ECMWF re-analysis	off-line ocean re-analysis product	http://cerawww.dkrz.de/WDCC/CMIP5/
MIROC5	-	integration using observational gridded ocean T and S	http://amaterasu.ees.hokudai.ac.jp/
MPI-ESM-LR	NCEP re-analysis	off-line ocean hindcast forced with NCEP	http://cerawww.dkrz.de/WDCC/CMIP5/

586

587 Table 3. Description of the six variables which contribute to the EASM. The abbreviation of these variables is followed to the guidelines of
588 CMIP5.

variable	Standard name	Contribution to the EASM
pr	Precipitation	Precipitation distribution indicates the strength of EASM
psl	Mean sea surface pressure	Differences of mean sea surface pressure between land and ocean lead to EASM
ua850	Zonal winds over 850 hPa	A component of low-level cyclone which transports vapor from ocean to land
va850	Meridional winds over 850 hPa	As ua850, and contributes to Hadley's cell
ua200	Zonal winds over 850 hPa	A component of upper-level Hadley's cell
va200	Meridional winds over 850 hPa	As ua200

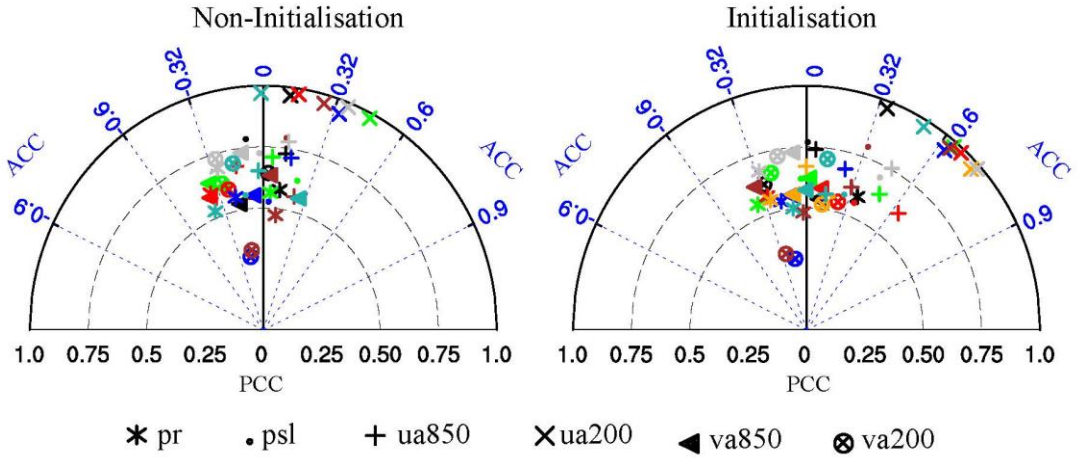

Fig.1. Taylor diagrams display of pattern (PCC) and temporal (ACC) correlation metrics of six variables between observation and model simulation in the EASM region (0-50ºN, 100-140ºE). Each coloured marker represents a model, *i.e.*, the BCC-CSM1-1 (black), the CanCM4 (green), the GFDL-CM2p1 (red), the HadCM3 (blue), the MIROC5 (brown), the MPI-ESM-LR (light-sea-blue), and the HadCM3-ff (orange). The GPCP was employed as the reference data for precipitation (*i.e.*, pr) while wind fields (*i.e.*, ua850, va850, ua200 and va200) and mean sea level pressure (*i.e.*, psl) were compared by ERA-Interim re-analysis.

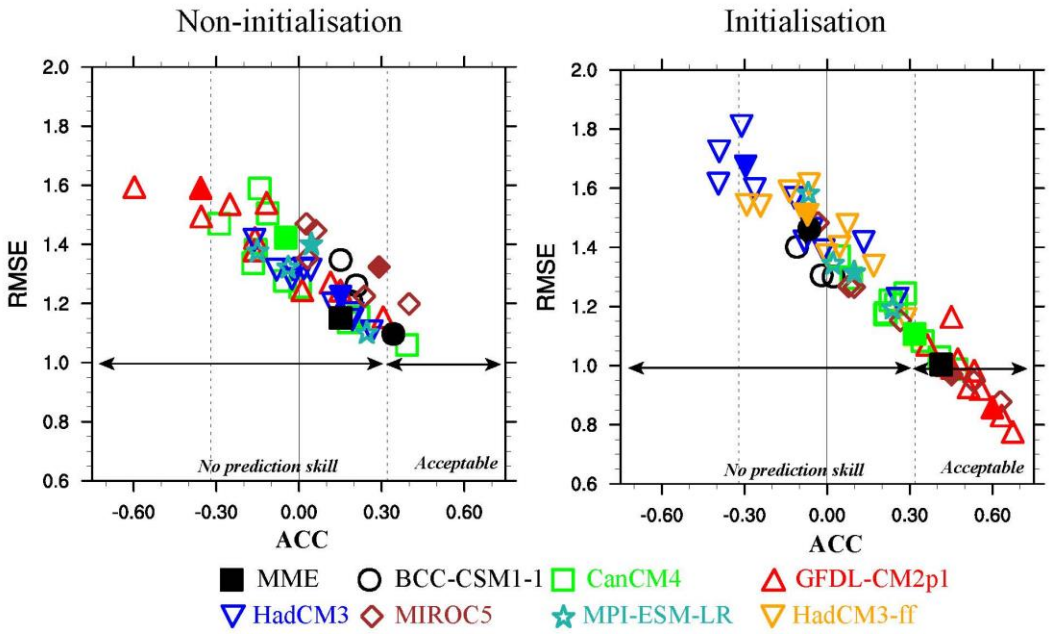

Fig. 2. Performance of the model ensemble member (hollow marker) and its ensemble mean (solid marker) on the EASM index. The abscissa and ordinates are the anomaly correlation coefficient (ACC) and the root-mean-square-error (RMSE), respectively. The observed EASM index is calculated by zonal wind at 850 hPa from the ERA-Interim re-analysis data. The black dot lines indicate the significant level at 0.1. The vertical black line represents the correlation between the simulating and the observational EASM index is 0.

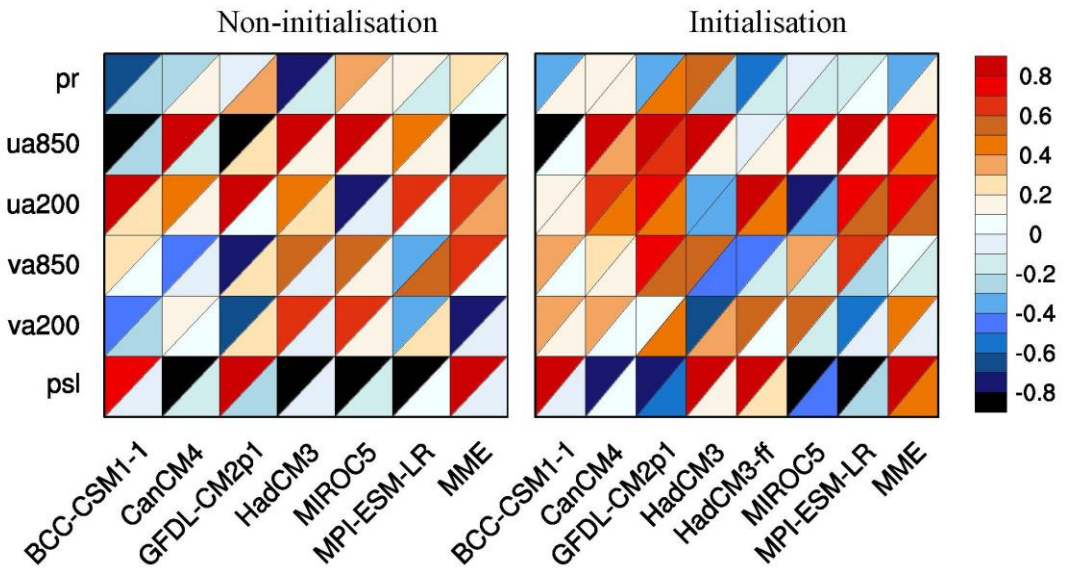

Fig. 3. Portrait diagram display of correlation metrics between the observation and the model simulation of the first lead EOF mode for the six fields in the non-initialisation (left) and the initialisation (right). Each grid square is split by a diagonal in order to show the correlation with respect to both the eigenvector (upper left triangle) and its associated principal components (lower right triangle) reference data sets.

620

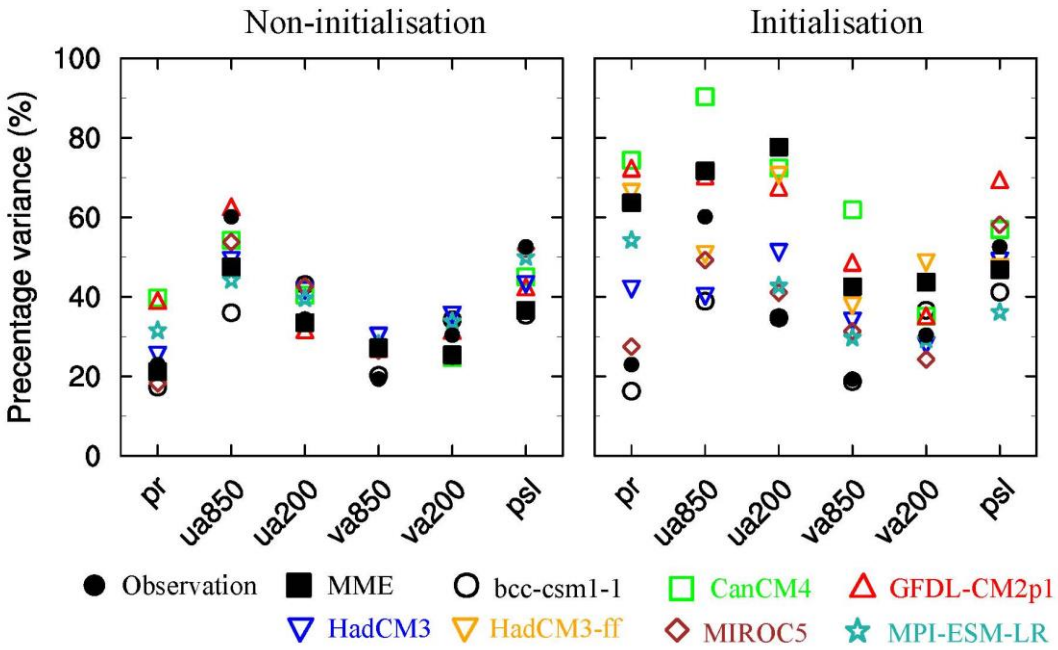

621

622 Fig. 4. Fraction variance (%) explained by the first EOF mode for six fields in the
623 non-initialisation (left) and the initialisation (right).

624

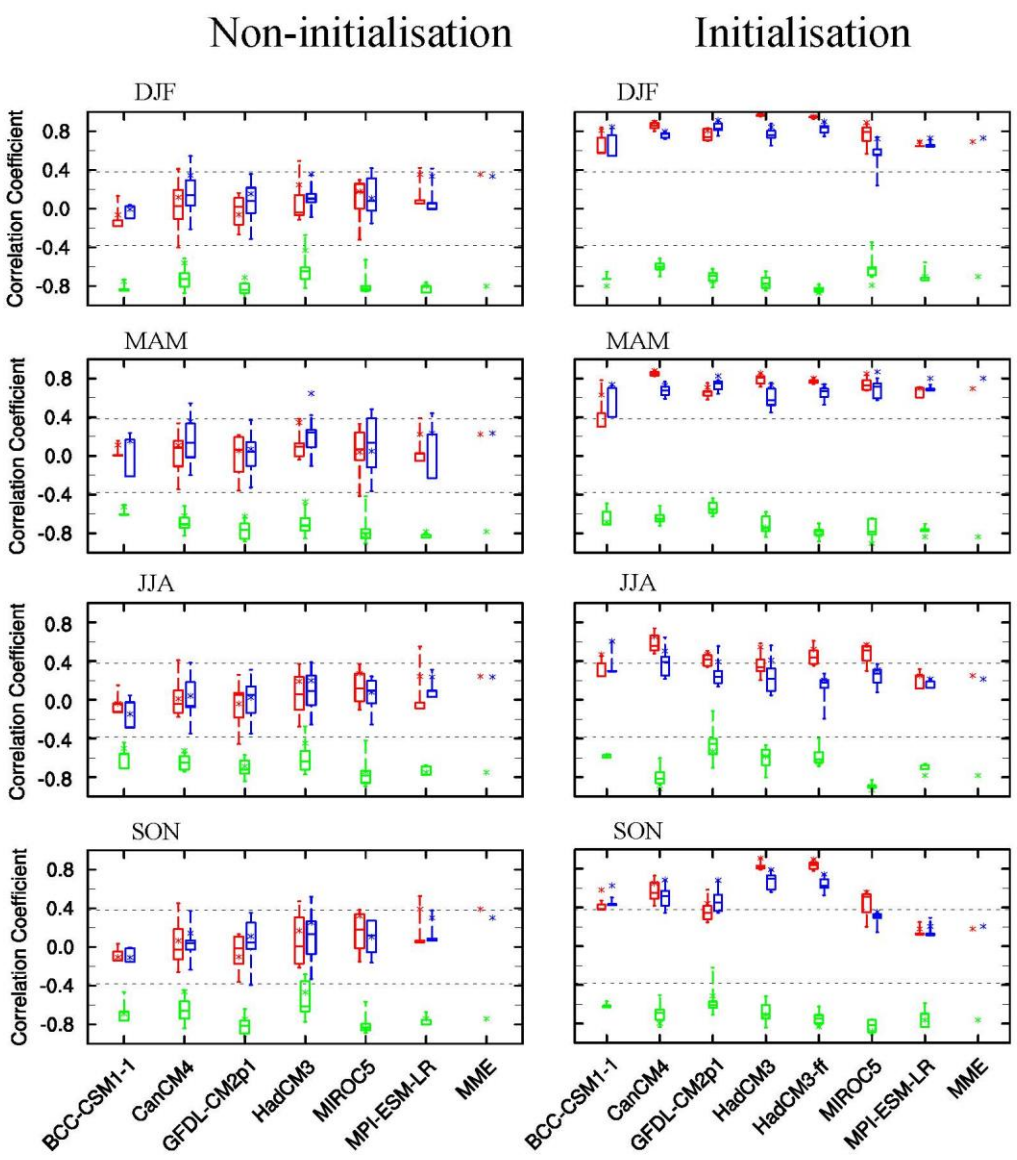

625

626 Fig. 5. Model prediction skill in representing the observational Niño3.4 (red), the SOI
627 (blue) from the DJF to SON in non-initialisation (left) and initialisation (right). Green
628 diagram shows the correlation coefficient between the model simulated Niño3.4 and
629 the SOI. Box and whisker diagram shows ensemble mean of each model (asterisk),
630 median (horizontal line), 25th and 75th percentiles (box), minimum and maximum
631 (whisker). The two black dotted lines indicate 0.05 significant level based upon
632 Student's t-test.

633

634

635

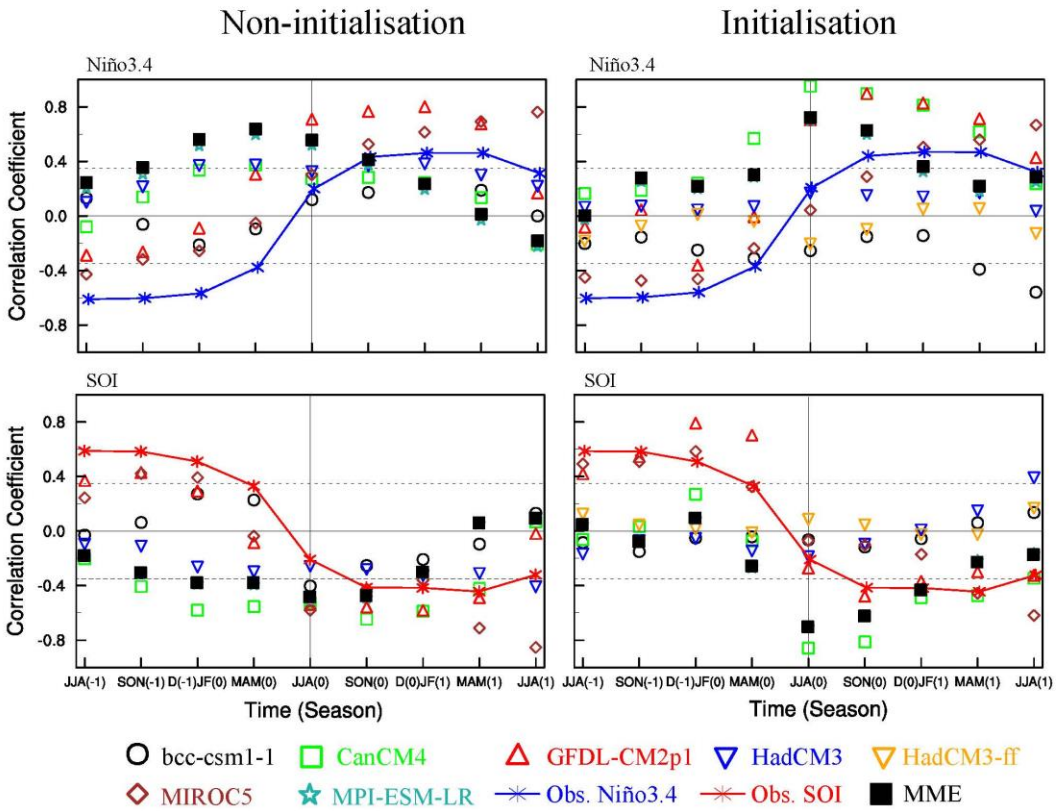

Fig. 6. Lead-lag correlation coefficients between the EASM index and Niño3.4 (upper), and SOI (lower) in non-initialised simulations (left) and initialised ones (right) for observation (marker line) and models (marker) from JJA(-1) to JJA(+1). The two black dotted lines are 0.05 significant level based upon Student's t-test. The vertical line represents JJA(0), where the simultaneous correlations between the EASM index and Niño3.4, and SOI are shown.